Dynamic Voltage Enhancement for Multi-Machine Power System Through PCH Based GCI

Madhumita Patil[1], Aakanksha Mane[2], Rayyan Petkar[3], Deepak Tiwari[4], Uday Suryawanshi[5], Sudhir Bhil[6], Sunny Kumar[7], Sushama Wagh[8]

***Abstract*—The recent trend of encouragement to renewable integration has resulted in an inverter-dominated hybrid grid. The time-scale of such integrated grid activities and its response time varies in a wide range. In such a scenario, the first challenge is to have a model that can capture both the dynamics of fast as well as slow components, and the second is stability analysis without compromising its time-varying impact. To address these issues, the paper includes the Port-Controlled Hamiltonian (PCH) Inverter formulation related to a interdisciplinary model for voltage stability analysis of inverter-dominated distribution grids. The interactions between slow network, load dynamics, intermediate converter-control dynamics, and fast electromagnetic states can be captured in the model. The PCH formulation provides an energy-based representation of the inverter dynamics, enabling systematic analysis of transient voltage response and post-disturbance recovery in inverter-integrated power systems. MATLAB is used to validate the proposed methodology in weak-grid and load-varying scenarios. A new PCH-based controller has been designed to tune the inverter PWM signal so that voltage stability can be supported to maintain the grid voltage profile.**

***Index Terms*—$\alpha\beta$ frame, Grid-Connected Inverter, Interconnection and Damping Assignment Passivity-Based Control (IDA-PBC), MATLAB/Simulink, Multimachine system, Port-controlled Hamiltonian (PCH), Voltage Source Inverter (VSI), Voltage stability**

I. INTRODUCTION

The power system is experiencing paradigm shift from an inertial-based architecture to a non-inertial converter-governed network. This transition is driven by the rapid penetration of inverter-interfaced renewable energy sources and electronically governed loads, which are replacing traditional rotating machines across the power system network. This results in remodeling of dynamic behavior, characterized by reduced inertia, limited inherent damping, and a growing dependence on power-electronics control to maintain system stability and operational reliability [1].

Inverter-based resources (IBRs) entirely rely on control algorithms to emulate voltage support and frequency regulation. This poses challenges related to voltage stability, oscillatory behavior, and post-disturbance voltage recovery in inverter-dominated grids. In particular, rotor angle stability and damping of interarea oscillations have become increasingly important in low-inertia systems [2], [3]. Furthermore, transient stability assessment and critical clearing time analysis remain important for evaluating system resilience under severe disturbances [4].

Energy-based approaches such as Port-Controlled Hamiltonian (PCH) modeling [5], [6] and passivity-based control (IDA-PBC) [7] have received significant attention in power electronics due to their ability to represent system dynamics in terms of stored energy, interconnection structure, and dissipation. By preserving system passivity, Hamiltonian formulations provide strong stability properties and clear physical insight into system behavior. Moreover, this framework offers a unified energy-based representation of the inverter, controller, network, and load dynamics, enabling systematic analysis of the interactions between inverter inner control loops, outer voltage or power regulation, network dynamics, and load behavior, which are often difficult to capture using conventional control approaches. Previous studies have demonstrated that passivity-based control strategies can improve the dynamic performance and robustness of grid-connected converters under non-ideal grid conditions [8].

Motivated by these challenges, the research evaluates a Hamiltonian-controlled inverter as a dynamic voltage support device in a multimachine system. The voltage source inverter is modeled using the Port-Controlled Hamiltonian (PCH) framework and controlled using the IDA-PBC methodology, enabling systematic energy shaping and damping injection. To assess the system-level impact of such an inverter, a representative IEEE 9-bus system topology is considered with an equivalent PV plant interfaced through the proposed Hamiltonian-controlled voltage support scheme inverter. The inverter is formulated in the dq reference frame and connected to the grid through an LCL filter.

The application of Hamiltonian-controlled inverter modeling in a multimachine system environment has not been widely reported in existing studies. While PCH modeling and IDA-PBC control have been previously applied to converter systems, their integration and comparative evaluation in a multimachine IEEE 9-bus environment for dynamic voltage support and transient stability analysis remains limited in existing literature.

The main contributions of this paper are summarized as follows:

- Integration of the Hamiltonian-controlled inverter into a multimachine system, enabling comparative evaluation of inverter-based voltage support.
- Comparative dynamic analysis of voltage, frequency, and rotor angle responses under grid disturbances for conven-

[1]Madhumita Patil is with E-MC^2, VJTI, Mumbai; [2]Aakanksha Mane is with E-MC^2, VJTI, Mumbai; [3]Rayyan Petkar is with E-MC^2, VJTI, Mumbai; [4]Deepak Tiwari is Sr Engineer, Comed, Chicago; [5]Uday Suryawanshi is with E-MC^2, VJTI, Mumbai; [6]Sudhir Bhil is with E-MC^2, VJTI, Mumbai; [7]Sunny Kumar is with E-MC^2, VJTI, Mumbai; [8]Sushama Wagh is with E-MC^2, VJTI, Mumbai, srwagh@ee.vjti.ac.in.

tional synchronous generator and Hamiltonian-controlled inverter configurations.

The subsequent sections focus on the strategy used for inverter modeling. Section III presents the development of the PCH framework for stability enhancement, while Section IV is dedicated to system description and case study. Section V presents the results and their interpretation. Section VI concludes the work along with future scope.

II. MATHEMATICAL MODELING OF GRID-CONNECTED INVERTER WITH PLL AND IDA-PBC

The mathematical model of the grid-connected inverter is developed using the Port-Controlled Hamiltonian (PCH) framework. The modeling procedure is carried out in a sequence of steps so that the energy variables, system dynamics, and control inputs can be systematically identified.

1) Step 1: Inverter–Filter Dynamic Equations: The inverter-side inductor, filter capacitor, and grid-side resistance dynamics are first expressed using Kirchhoff's laws in the stationary $\alpha\beta$ reference frame. The following dynamic equations are adapted from the Port-Controlled Hamiltonian modeling approach presented in [5]. The resulting differential equations are given in (1)–(5):

$$L_f \dot{i}_{L\alpha} = -R_f i_{L\alpha} + \omega L_f i_{L\beta} - v_{C\alpha} + v_{\text{inv},\alpha}, \quad (1)$$

$$L_f \dot{i}_{L\beta} = -R_f i_{L\beta} - \omega L_f i_{L\alpha} - v_{C\beta} + v_{\text{inv},\beta}, \quad (2)$$

$$C_f \dot{v}_{C\alpha} = \omega C_f v_{C\beta} + i_{L\alpha} - \frac{v_{C\alpha}}{R_L}, \quad (3)$$

$$C_f \dot{v}_{C\beta} = -\omega C_f v_{C\alpha} + i_{L\beta} - \frac{v_{C\beta}}{R_L}, \quad (4)$$

$$C_{\text{dc}} \dot{V}_{\text{dc}} = -(\mu_1 i_{L\alpha} + \mu_2 i_{L\beta}), \quad (5)$$

where $v_{\text{inv},\alpha} = \mu_1 V_{\text{dc}}$ and $v_{\text{inv},\beta} = \mu_2 V_{\text{dc}}$ represent the inverter modulation voltages.

2) Step 2: Hamiltonian Energy Function: The total stored electromagnetic energy of the inverter–filter system is represented through the Hamiltonian function. The Hamiltonian is defined as

$$H = \frac{1}{2}L_f(i_{L\alpha}^2 + i_{L\beta}^2) + \frac{1}{2}C_f(v_{C\alpha}^2 + v_{C\beta}^2) + \frac{1}{2}C_{\text{dc}}V_{\text{dc}}^2. \quad (6)$$

The corresponding state vector of the system is

$$x = [\, i_{L\alpha},\ i_{L\beta},\ v_{C\alpha},\ v_{C\beta},\ V_{\text{dc}}\,]^T. \quad (7)$$

3) Step 3: Port-Controlled Hamiltonian Representation: Using the Hamiltonian defined in (6), the system dynamics given in (1)–(5) can be expressed in the compact PCH form

$$\dot{x} = [J - R]\nabla H + g(x)u. \quad (8)$$

Here, J represents the skew-symmetric interconnection matrix and R denotes the dissipation matrix describing system losses. The matrices are defined as

$$J = \begin{bmatrix} 0 & \omega L_f & -1 & 0 & 0 \\ -\omega L_f & 0 & 0 & -1 & 0 \\ 1 & 0 & 0 & \omega C_f & 0 \\ 0 & 1 & -\omega C_f & 0 & 0 \\ 0 & 0 & 0 & 0 & 0 \end{bmatrix}$$

$$R = \begin{bmatrix} R_f & 0 & 0 & 0 & 0 \\ 0 & R_f & 0 & 0 & 0 \\ 0 & 0 & \frac{1}{R_L} & 0 & 0 \\ 0 & 0 & 0 & \frac{1}{R_L} & 0 \\ 0 & 0 & 0 & 0 & 0 \end{bmatrix}.$$

The input vector and port matrix are expressed as

$$u = \begin{bmatrix} \mu_1 \\ \mu_2 \end{bmatrix}, \qquad g(x) = \begin{bmatrix} V_{\text{dc}} & 0 \\ 0 & V_{\text{dc}} \\ 0 & 0 \\ 0 & 0 \\ -i_{L\alpha} & -i_{L\beta} \end{bmatrix}.$$

The passivity property of the system follows from the Hamiltonian derivative

$$\dot{H} = -(\nabla H)^T R \nabla H + (\nabla H)^T g u. \quad (9)$$

4) Step 4: IDA-PBC Control Law: The Interconnection and Damping Assignment Passivity-Based Control (IDA-PBC) method reshapes the system energy and introduces damping to guarantee closed-loop stability. The controlled dynamics can be written as

$$\dot{x} = (J_d - R_d)\nabla H_d. \quad (13)$$

In the IDA-PBC formulation, J_d defines the desired interconnection structure of the closed-loop system, whereas R_d determines the desired damping injection required to dissipate system energy and suppress oscillatory behavior.

The corresponding modulation inputs are obtained as

$$\begin{bmatrix} \mu_1 \\ \mu_2 \end{bmatrix} = \frac{1}{V_{\text{dc}}}\left[-R_f i_L + v_C + K_p(v_C^{ref} - v_C) + K_i(i_L^{ref} - i_L)\right]. \quad (14)$$

The modulation inputs obtained from the IDA-PBC controller represent the normalized inverter voltage references in the stationary $\alpha\beta$ frame. Accordingly, the inverter output voltages are expressed as

$$v_{inv,\alpha} = \mu_1 V_{dc} \quad (1)$$

$$v_{inv,\beta} = \mu_2 V_{dc} \quad (2)$$

These reference voltages are transformed into three-phase modulation voltages using the inverse Clarke transformation to obtain v_{abc}. The resulting phase voltages are then normalized with respect to the DC-link voltage in order to generate the PWM duty ratios required for inverter switching.

5) Step 5: PWM Generation and Power Computation: The modulation signals are converted to three-phase duty ratios using

$$d_{abc} = 0.5 + \frac{v_{abc}}{V_{\text{dc}}}. \tag{15}$$

The instantaneous active and reactive power exchanged with the grid are computed as

$$P = \frac{3}{2}(v_\alpha i_{L\alpha} + v_\beta i_{L\beta}), \tag{16}$$
$$Q = \frac{3}{2}(v_\beta i_{L\alpha} - v_\alpha i_{L\beta}). \tag{17}$$

III. DEVELOPMENT OF PCH FRAMEWORK FOR ENHANCEMENT OF STABILITY

Based on the dynamic equations and the PCH representation derived in the previous section, the overall control architecture of the grid-connected inverter is implemented for system-level operation in the multimachine network. The interaction among the various subsystem blocks is illustrated in Fig. 1, highlighting the overall control and power flow.

The three-phase grid voltages are first measured (Step 1) and converted through a Clarke transform (Steps 2–3). These signals, together with the DC-link voltage, are processed by the IDA-PBC Hamiltonian controller to generate the required inverter voltage references (Step 4). The references are then mapped back to three-phase quantities using the inverse Clarke transform (Step 5), converted into PWM duty ratios (Step 6), and compared with a carrier signal to produce switching pulses for the universal bridge (Step 7). The bridge output is filtered through the LCL network (Step 8) to ensure smooth current injection before being delivered to the multimachine power system (Step 9). Grid currents and voltages are continuously measured to complete the feedback loop and maintain closed-loop operation.

Conventional inverter control methods generally suppress oscillations using externally designed feedback damping loops. However, in the proposed Hamiltonian framework, damping is systematically introduced through passivity-based energy shaping and dissipation assignment.

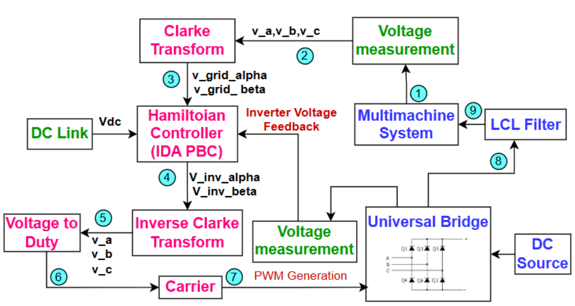

Fig. 1. Workflow diagram of a multimachine system with a Hamiltonian-based inverter.

TABLE I
INVERTER AND LCL FILTER PARAMETERS

Parameter	Value
Inverter-side inductance L_f	2 mH
Filter resistance R_f	0.1 Ω
Filter capacitance C_f	5×10^{-3} F
Load resistance R_L	10 Ω
DC-link capacitance C_{dc}	2×10^{-3} F
DC-link voltage V_{dc}	600 V
Grid frequency f	50 Hz
Angular frequency ω	$2\pi \times 50$ rad/s

IV. SYSTEM DESCRIPTION AND CASE STUDY

Fig. 2 shows the single-line diagram (SLD) of the modified IEEE 9-bus system, highlighting the placement of the Hamiltonian-controlled inverter at Bus 3 and the location of the three-phase LLL fault considered near Bus 7.

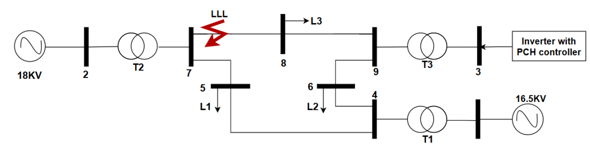

Fig. 2. Single-line diagram of the modified IEEE 9-bus system with inverter integration.

In order to evaluate the effectiveness of the proposed Hamiltonian-based control strategy, three different system configurations are considered for comparison. The grid-following inverter with PI control represents the conventional inverter control approach widely used in practical renewable energy applications, whereas the Hamiltonian-controlled inverter is considered to investigate the effectiveness of the IDA-PBC framework in improving dynamic stability and voltage support performance.

- **Case 1:** Conventional generator-based system.
- **Case 2:** Grid-following inverter using PI control.
- **Case 3:** Hamiltonian-controlled inverter using the IDA-PBC framework.

This section presents a comparative dynamic assessment of a multimachine system adapted from the IEEE 9-bus system under different inverter integration and control scenarios. A three-phase fault is considered near Bus 7 at $t = 2$ sec and cleared at $t = 2.1$ sec. Voltage magnitude and system frequency are monitored at Bus 3 to evaluate voltage support capability and frequency behavior during both healthy and disturbed operating conditions.

1) Case 1 (Conventional Generator-Based System): Fig. 3 shows the voltage response at Bus 3 when an LLL-fault is considered near Bus 7. Under pre-fault conditions, the voltage is maintained at approximately 1.03 pu. During the fault interval (2–2.1 sec), the voltage drops sharply to 0.4 pu, corresponding to a 61.1% voltage dip. After fault clearance, a post-fault voltage overshoot is observed, with the voltage rising to approximately 1.08 pu before settling back to its nominal value of 1.03 pu. This represents a post-fault voltage spike of approximately 4.85% from the initial value.

The corresponding frequency response is shown in Fig. 4. During the fault, the frequency increases from 60 Hz to

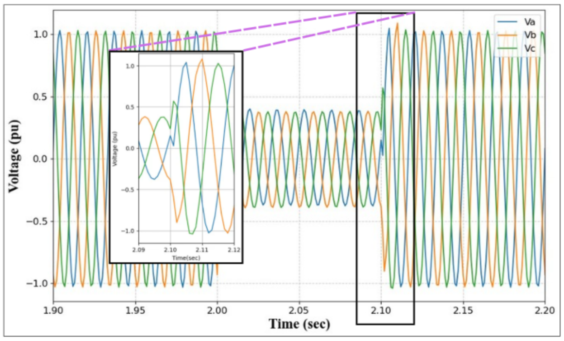

Fig. 3. Voltage at Bus 3 during LLL-fault with generator in IEEE 9-bus system.

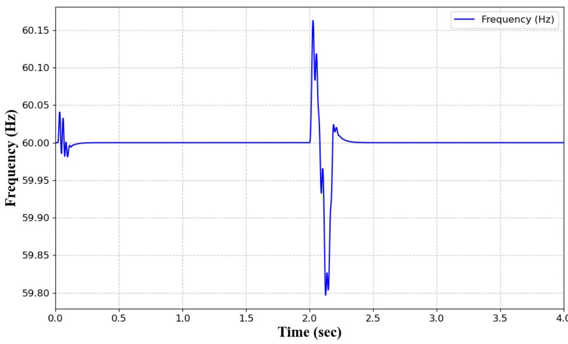

Fig. 4. Frequency response for LLL-fault in IEEE 9-bus system.

approximately 60.15 Hz, followed by a dip to 59.80 Hz after fault clearance. The frequency subsequently recovers and settles at the nominal value of 60 Hz.

2) Case 2 (Grid-Following Inverter With PLL Using PI Control): The PI controller parameters were selected using conventional tuning practices to ensure stable grid-following operation under nominal conditions.

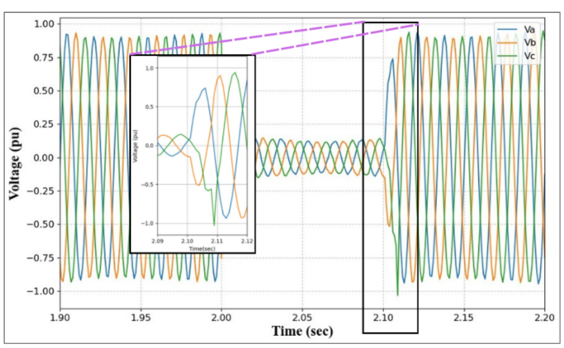

Fig. 5. Voltage at Bus 3 during LLL-fault (grid-following VSI).

During the LLL-fault, the voltage response shown in Fig. 5, considering the operating scenario the pre-fault voltage is observed to be 0.92 pu that drops to nearly 0.12 pu, corresponding to an 86.9% voltage dip. Following fault clearance, an additional voltage change is observed, with the voltage momentarily reaching approximately -1.03 pu, which is an 11.9% change before recovering to its pre-fault value. The frequency response during the fault is shown in Fig. 6; the

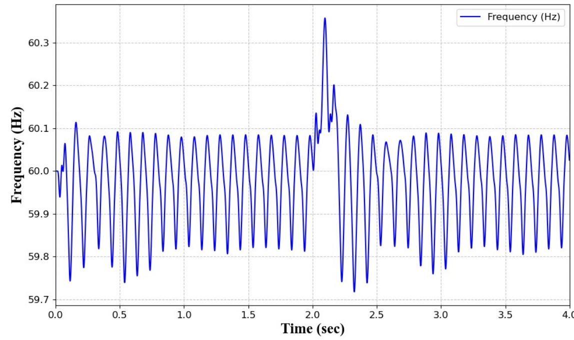

Fig. 6. Frequency response during LLL fault (grid-following VSI).

frequency spikes to approximately 60.39 Hz during the fault and then returns to the same oscillatory behavior observed under healthy conditions, ranging between 59.8 Hz and 60.1 Hz.

3) Case 3 (Hamiltonian-Controlled Inverter Using the IDA-PBC Framework): For the Hamiltonian-controlled inverter, the voltage response is shown in Fig. 7; the initial voltage is 0.93 pu and has a smooth and stable three-phase voltage supply. The corresponding frequency response in Fig. 8 remains tightly regulated at 60 Hz, indicating improved steady-state behavior compared to the grid-following inverter with PI controller.

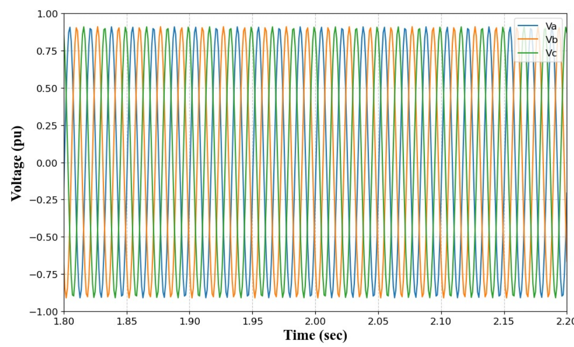

Fig. 7. Voltage at Bus 3 under healthy conditions (Hamiltonian-controlled VSI).

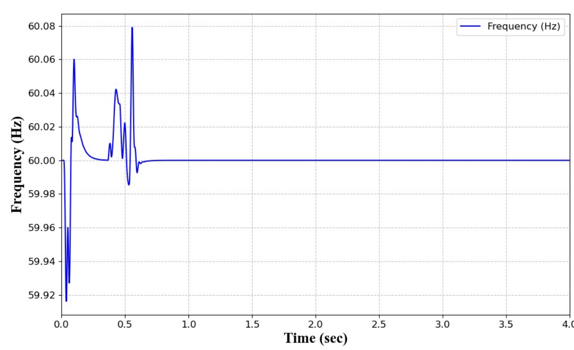

Fig. 8. Frequency response under healthy conditions (Hamiltonian-controlled VSI).

During the LLL-fault, the voltage at Bus 3 shown in Fig. 9 drops to approximately 0.125 pu, corresponding to an 86.5% voltage dip. After fault clearance, the voltage recovers smoothly with a limited overshoot to approximately 0.956 pu

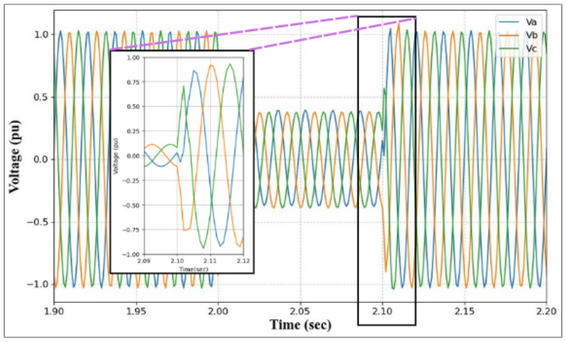

Fig. 9. Voltage at Bus 3 during LLL-fault (Hamiltonian-controlled VSI).

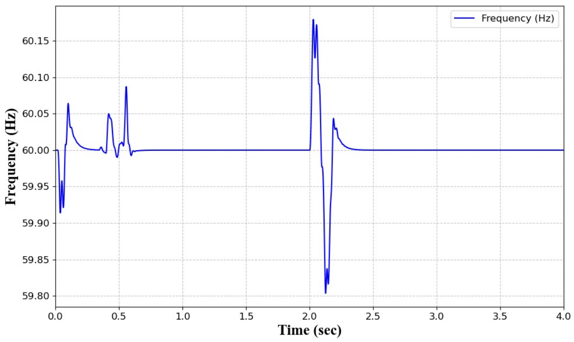

Fig. 10. Frequency response during LLL-fault (Hamiltonian-controlled VSI).

before settling back to its pre-fault value. This corresponds to a post-fault voltage spike of only 2.81%.

The frequency response during the fault, shown in Fig. 10, exhibits a limited deviation, with a maximum increase to approximately 60.17 Hz and a minimum of 59.8 Hz. Following fault clearance, the frequency rapidly returns to the nominal value of 60 Hz without sustained oscillations. Although voltage dynamics are strongly influenced by the inverter controller, the overall system frequency is mainly regulated by the collective dynamics of the interconnected grid, resulting in comparatively smaller frequency deviations.

TABLE II
COMPARISON OF DYNAMIC RESPONSES UNDER LLL FAULT

System Configuration	**Voltage Dip**	**Post-Fault Overshoot**	**Frequency Deviation**
Conventional Generator System	61.1%	4.85%	+0.15 Hz / -0.20 Hz
Grid-Following Inverter (PLL + PI Control)	86.9%	11.9%	+0.39 Hz / -0.20 Hz
Hamiltonian-Controlled Inverter (IDA-PBC)	86.5%	2.81%	+0.17 Hz / -0.20 Hz

V. CONCLUSIONS

Effective dynamic voltage support is demonstrated through the integration of a Hamiltonian-controlled inverter in a multi-machine power system. A comparative system-level study was conducted on the adapted IEEE 9-bus network to evaluate voltage and frequency behavior under a three-phase LLL fault near Bus 7. The performance of three configurations was analyzed: a conventional generator-based system, a grid-following inverter with PLL-based cascaded PI control, and a Hamiltonian-controlled inverter based on the IDA-PBC framework.

The results show that the Hamiltonian-controlled inverter provides improved transient voltage support compared to the other configurations. It achieves faster post-fault voltage recovery and significantly reduced voltage overshoot, with nearly 42% lower overshoot than the generator-based case. Frequency deviations are also better damped with rapid convergence to the nominal value. Additional simulations with faults at different network locations exhibit similar trends, indicating consistent performance. These findings highlight the potential of Hamiltonian-based control for enhancing dynamic voltage support in inverter-integrated power systems.

ACKNOWLEDGMENT

Authors are grateful for the rigorous technical discussions of Prof. Navdeep M. Singh (IGI Research Chair Professor, VJTI). The authors would also like to acknowledge the Lab facilities provided by SAVEX Sponsored E-MC^2 Lab, VJTI, Mumbai and the financial support extended by IGI Pvt. Ltd to conduct the research activities.

REFERENCES

[1] J. Liu, F. Blaabjerg, and D. M. Vilathgamuwa, "Review of Grid-Forming Inverter Technologies for Renewable Energy Integration," *IEEE Access*, vol. 8, pp. 132489–132508, 2020.

[2] K. Sunny, A. Sheikh, and S. Wagh, "Dynamic Mode Decomposition for Prediction and Enhancement of Rotor Angle Stability," in *Proc. 2020 7th International Conference on Control, Decision and Information Technologies (CoDIT)*, 2020, pp. 1–6.

[3] C. Wagh, D. Bhurawalla, S. Chaurasia, Y. Shaikh, V. Shinde, K. Sunny, and S. Bhil, "Damping Interarea Oscillations in Hybrid Grid," in *Proc. 2022 IEEE PES 14th Asia-Pacific Power and Energy Engineering Conference (APPEEC)*, 2022, pp. 1–5.

[4] J. P. Narayan, S. Kumar, M. Patil, P. Goswami, P. Pentayya, and F. Kazi, "Study on Critical Clearing Time of Mumbai Grid Based on Dynamic Simulation," in *Proc. 2022 4th International Conference on Energy, Power and Environment (ICEPE)*, 2022, pp. 1–6.

[5] R. V. Meshram, M. Bhagwat, S. R. Wagh, and N. M. Singh, "Port-Controlled Phasor Hamiltonian Modeling and IDA-PBC Control of Solid-State Transformer," *IEEE Transactions on Control Systems Technology*, vol. 25, no. 6, pp. 2141–2153, Nov. 2017.

[6] R. V. Meshram, S. V. Khade, S. R. Wagh, N. M. Singh, and A. M. Stanković, "Bond Graph Approach for Port-Controlled Hamiltonian Modeling for SST," *Electric Power Systems Research*, vol. 158, pp. 105–114, 2018.

[7] R. Ortega, A. van der Schaft, B. Maschke, and G. Escobar, "Interconnection and Damping Assignment Passivity-Based Control of Port-Controlled Hamiltonian Systems," *Automatica*, vol. 38, no. 4, pp. 585–596, Apr. 2002.

[8] F. M. Serra, C. H. De Angelo, and D. G. Forchetti, "IDA-PBC Controller Design for Grid-Connected Front-End Converters Under Non-Ideal Grid Conditions," *Electric Power Systems Research*, vol. 142, pp. 12–19, 2017.